SAND2013-10257P

*Exceptional service in the national interest*

Sandia National Laboratories

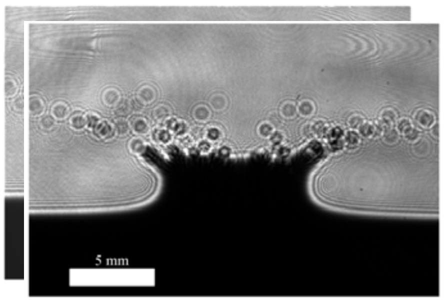


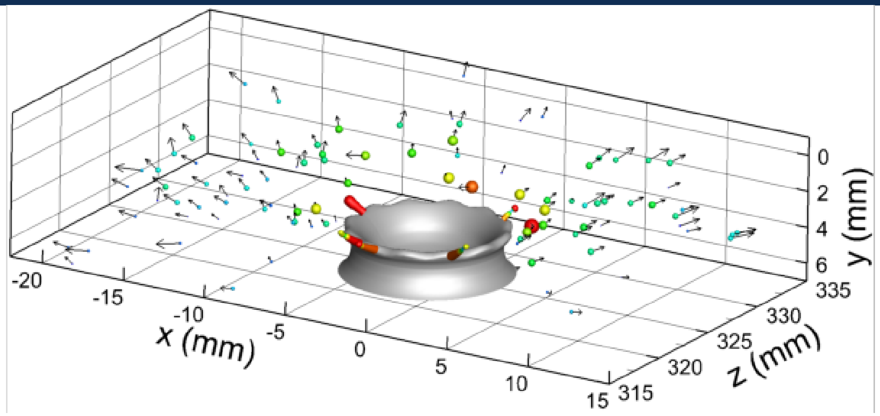


# Developments in digital holography enable the measurement of three-dimensional particle fields with improved accuracy

*CRF Research Highlight Series*


Daniel R. Guildenbecher (1512)


December 5, 2013

U.S. DEPARTMENT OF ENERGY

NNSA National Nuclear Security Administration


Sandia National Laboratories is a multi-program laboratory managed and operated by Sandia Corporation, a wholly owned subsidiary of Lockheed Martin Corporation, for the U.S. Department of Energy's National Nuclear Security Administration under contract DE-AC04-94AL85000.

# Motivation: 3D imaging for a 3D world

Challenge: 2D imaging or point-wise measurements cannot resolve 3D flow phenomena

- Experimental repetition needed to capture spatial statistics

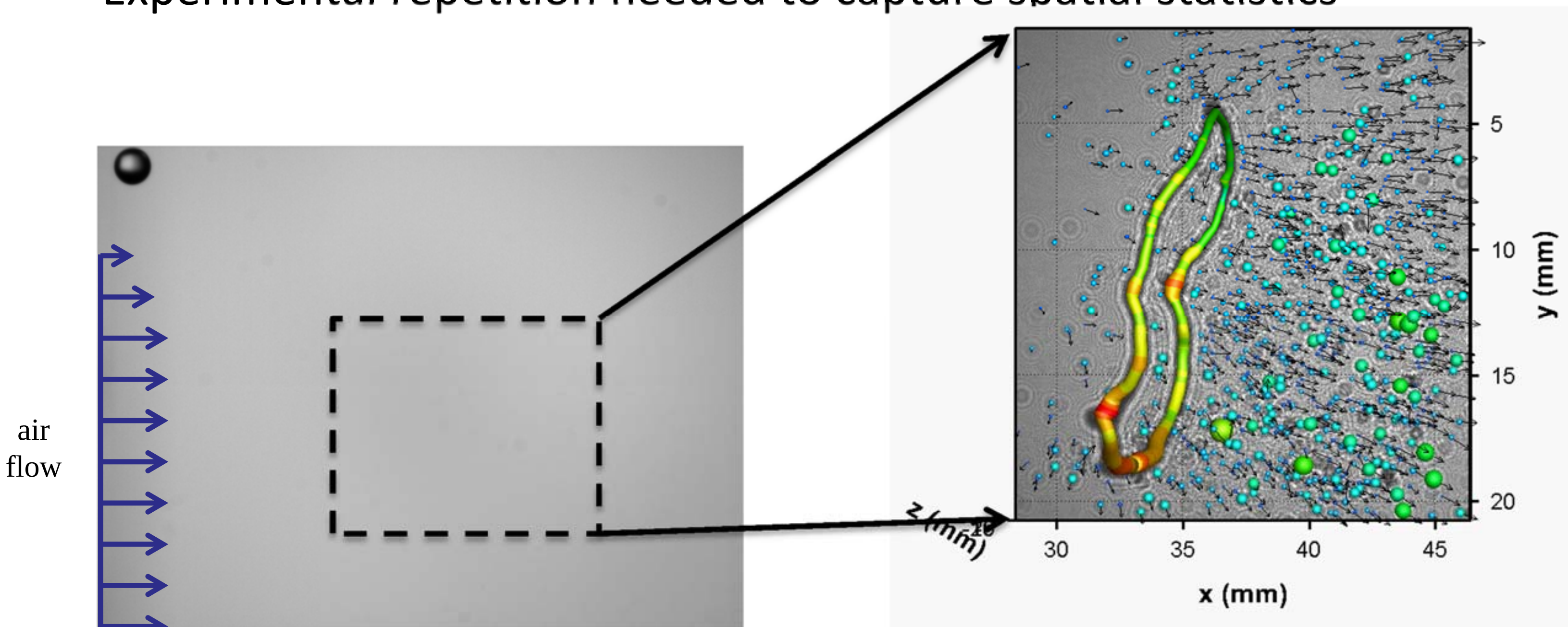


high-speed video of a ethanol drop in an air-stream

digital holographic measurement (Gao, Guildenbecher et al, 2013, *Opt. Lett.*)

**Holography is an optical technique to record and reconstruct a 3D light field**

- SNL applications include sprays, high-speed particle fields, fluid-flow measurements, droplet combustion, etc…

# What is holography?

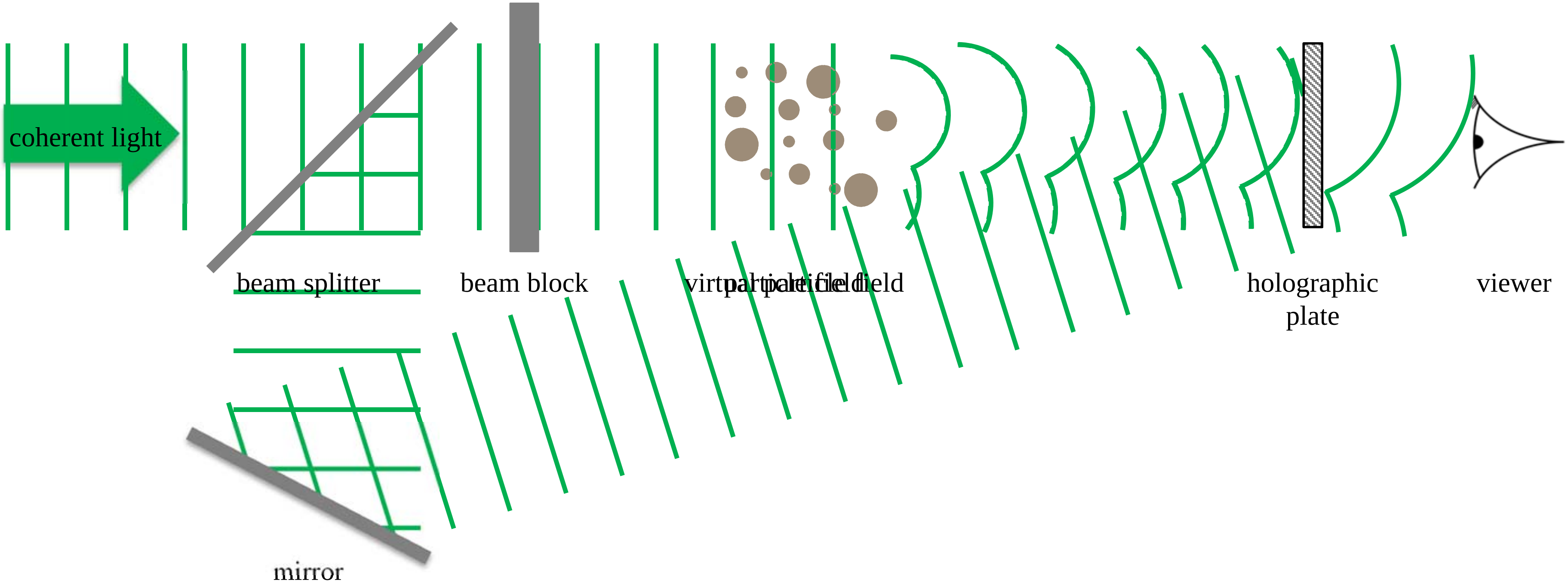


Optical method first proposed by Gabor in 1948

1. Coherent light scattered by particle field forms the object wave, $E_o$
2. Interference with a reference wave, $E_r$, forms the hologram: $h = |E_o + E_r|^2$
3. Reconstruction with $E_r$ forms virtual images at original particle locations

$$h \cdot E_r = \underbrace{(|E_o|^2 + |E_r|^2)E_r}_{\text{DC term}} + \underbrace{|E_r|^2 E_o}_{\text{virtual image}} + \underbrace{E_r^2 E_o^*}_{\text{real image}}$$

# Digital in-line holography (DIH)

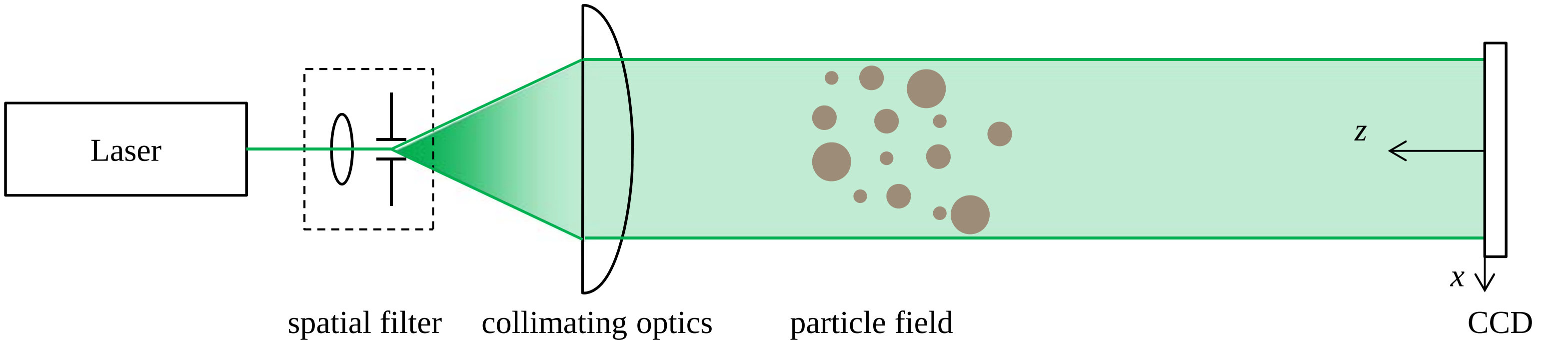


Holographic plate and cumbersome wet-chemical processing replaced with digital sensor (CCD or CMOS)

- Resolution of digital sensors (order 100 line pairs/mm) is much less than resolution of photographic emulsions (order 5,000 line pairs/mm)
  - For suitable off axis angles, $\theta$, the fringe frequency, $f$, is typically too large to resolve with digital sensors ($f = 2\sin(\theta/2)/\lambda$)
- Rather, the in-line configuration ($\theta = 0$) is typically utilized
  - Reference wave is that portion of the beam which passes through the particle field undisturbed
  - **Consequently, the real image overlaps with an out-of-focus virtual image**

# Digital in-line holography (DIH)

- In the computer, we multiply the digitally recorded hologram *h* by an estimate of the complex conjugate of the reference wave $E_r$*

$$h \cdot E_r^* = \underbrace{(|E_o|^2 + |E_r|^2)E_r^*}_{\text{DC term}} + \underbrace{E_r^{*2}E_o}_{\text{virtual image}} + \underbrace{|E_r|^2 E_o^*}_{\text{real image}}$$

- This complex amplitude can be numerically propagated to any distance along the optical axis, z, using the diffraction equations

$$E(x,y,z) = h(x,y) \cdot E_r^*(x,y) \otimes g(x,y,z)$$

  - Rayleigh-Sommerfeld: $g(x,y,z) = e^{jk\sqrt{x^2+y^2+z^2}} \Big/ j\lambda\sqrt{x^2+y^2+z^2}$
  - Fresnel-Kirchhoff: $g(x,y,z) = \dfrac{e^{jkz}}{j\lambda z} e^{jk\left(x^2+y^2\right)/2z}$

- Numerically, the convolution is computed using the fast Fourier transform (FFT)

$$E(x,y,z) = FFT^{-1}\left\{FFT\left\{I_0(x,y)E_r^*(x,y)\right\}FFT\left\{g(x,y,z)\right\}\right\}$$

- Visualized via the reconstructed amplitude, $A = |E|$, or intensity, $I = |E|^2$

# Digital in-line holography (DIH)

Sandia National Laboratories

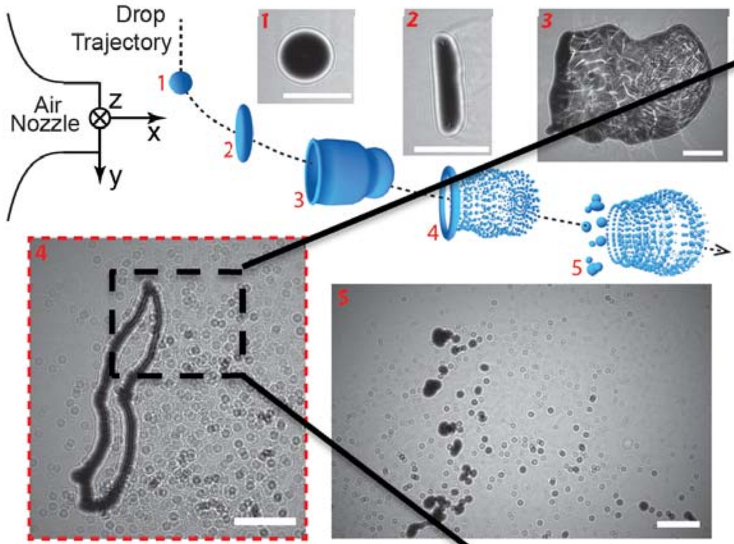


digital holograms of the breakup of an ethanol drop in an air-stream (Gao, Guildenbecher et al 2013, *Opt. Lett.*)

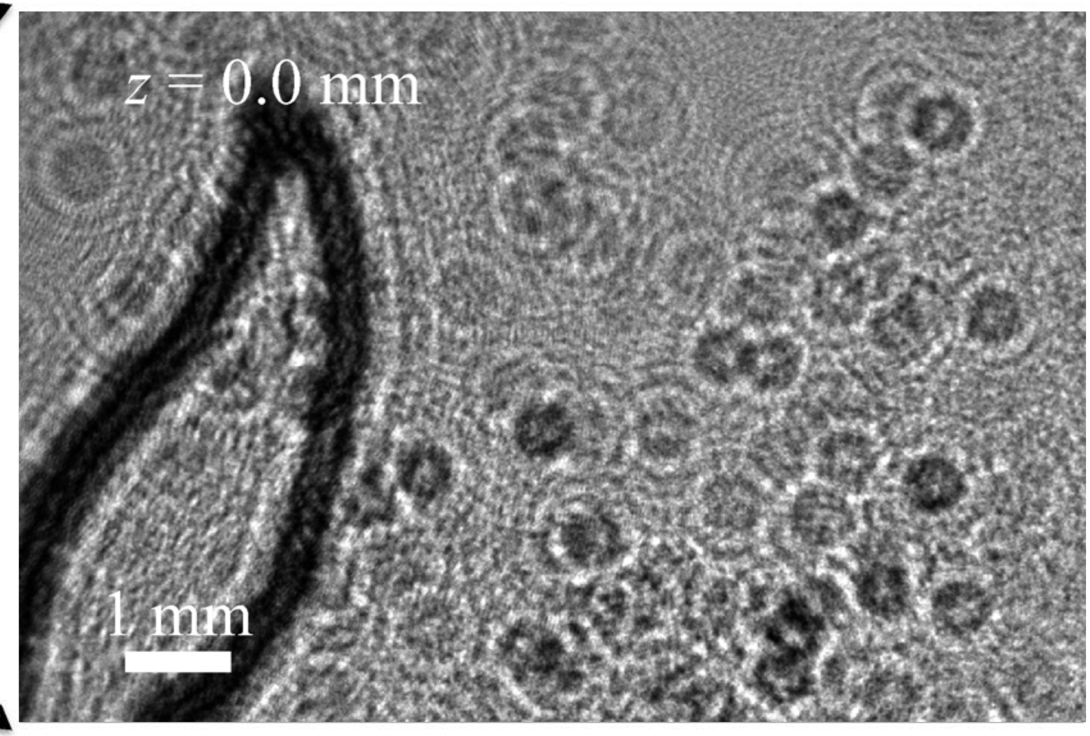


Reconstructed amplitude throughout depth, *z*

- In-focus structures are clearly observed at different depths, *z*
- "Rings" around the in-focus structures are the out-of-focus virtual images

**Challenge: How can we automatically extract in-focus objects?**

# The depth-of-focus problem

The spatial extent of the diffraction pattern limits the angular aperture, $\Omega$, from which a particle is effectively reconstructed (Meng et al, 2004, *Meas. Sci. Technol.*):

- From the central diffraction lobe → $\Omega \approx 2\lambda/d$
- Using the traditional definition of depth-of-focus, $\delta$, based on change of intensity within the particle center → $\delta \approx 4\lambda/\Omega^2$
- Therefore: for in-line holography, $\delta \approx d^2/\lambda$
  - Example: $d$ = 465 μm, $\lambda$ = 532 nm → $\delta \approx$ 400 mm!

Literature contains two basic methods to find the focal plane with improved accuracy:

1. Fit a model to the observed diffraction patterns (inverse method)
   - Generally accurate with small depth uncertainty
   - Limited to objects with known diffraction patterns (spheres)
2. Reconstruct the amplitude (or intensity) throughout depth and apply a focus metric to find "in-focus" objects
   - No *a-priori* knowledge of particle shape required
   - Accuracy is a strong function of the chosen focus metric

# Hybrid particle extraction method

<u>Basic idea:</u> In-focus regions display a minimum amplitude within the particle interior and a maximum sharpness at the particle edges

- Validity of this assumption has been verified through simulation

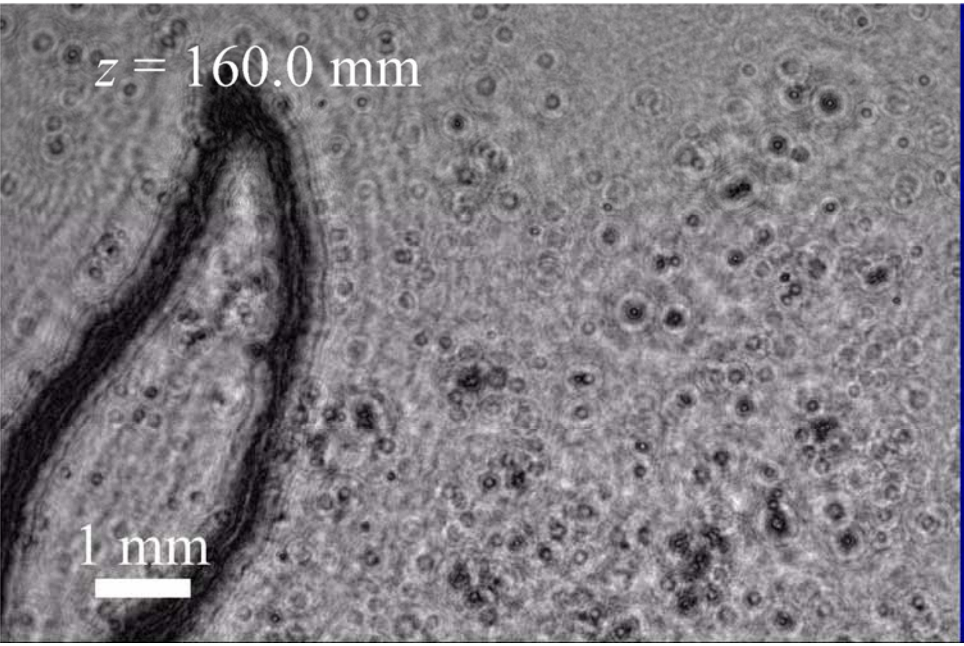


Reconstructed amplitude throughout depth, *z*

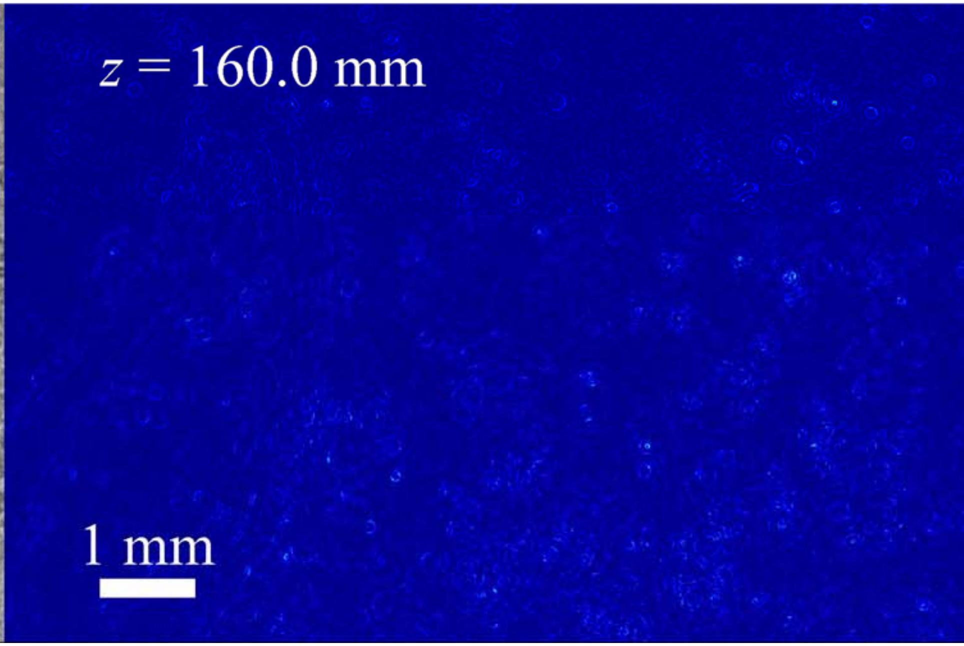


Reconstructed edge sharpness throughout depth, *z*

- Optimum threshold for particle extraction is automatically extracted from the threshold of the amplitude which displays maximum edge sharpness
  - Further details in Guildenbecher et al, 2013, *Appl. Opt.* and Gao, Guildenbecher, et al, 2013, *Opt. Express.*

# Experimental validation

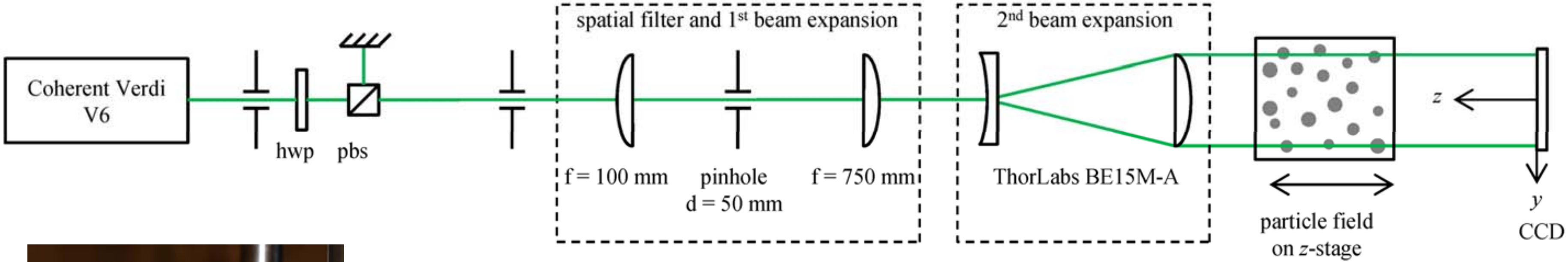


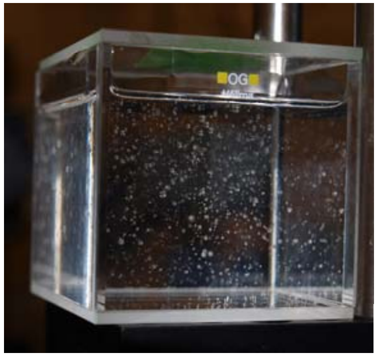

particle field

- Quasi-stationary particle field
  - Polystyrene beads ( $\bar{d} \approx 465\,\mu\text{m}$ ) in 10,000 cSt silicone oil
  - Settling velocity ≈ 0.8 mm/s
- Multiple holograms recorded, displacing the particle field 2 mm in the z-direction between each acquisition

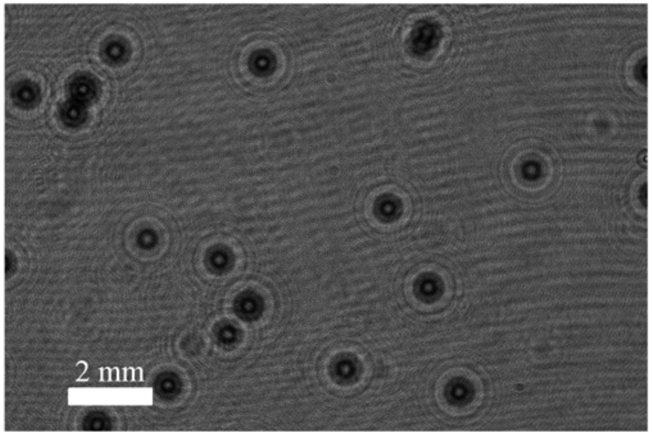


hologram

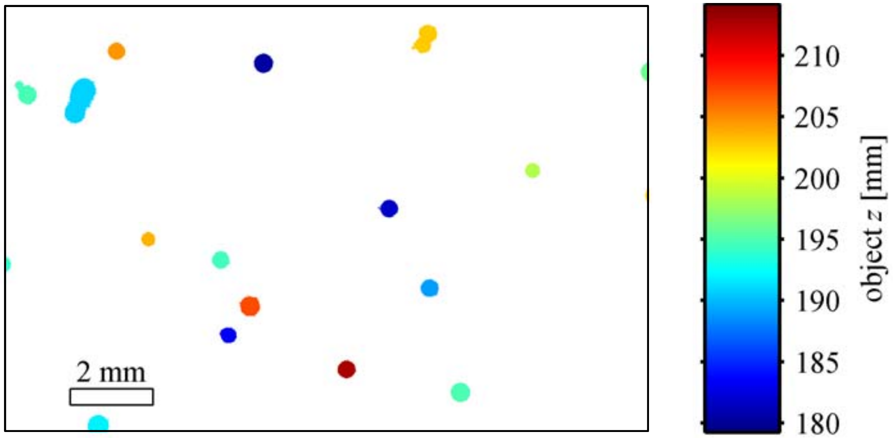


Detected objects colored by z-position

# Experimental validation

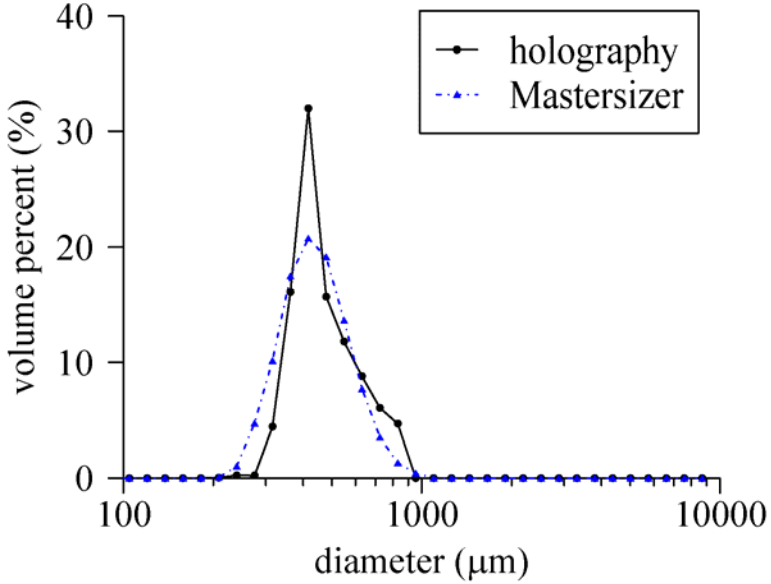


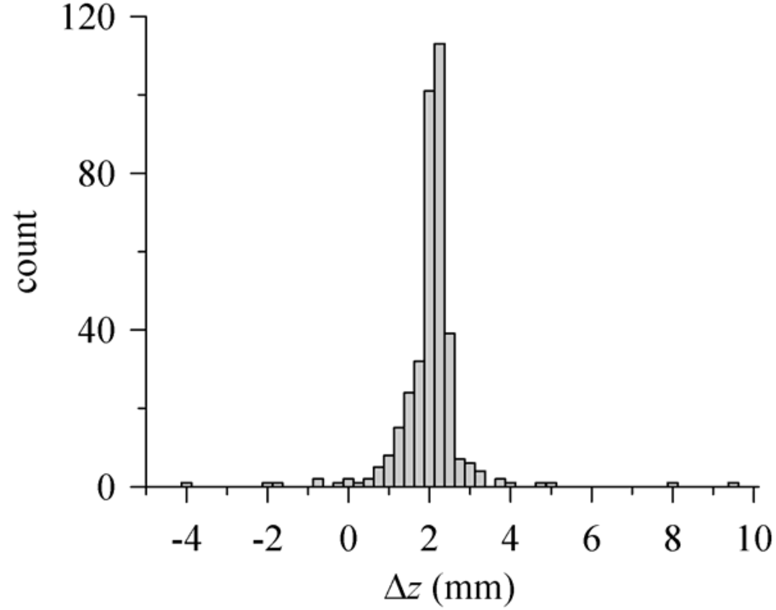


Diameter measured from area of the detected 2D morphology

- Actual mass median diameter = 465 μm
- Measured mass median diameter = 474 μm
  - Error of 2.0% with respect to actual value

Displacement found by particle matching between successive holograms

- Actual displacement = 2.0 mm
- Mean detected displacement = 1.91 mm +/- 0.81 mm
  - Standard deviation of 1.74 times mean diameter

# Aerodynamic drop fragmentation

Motivation: fundamental spray process and an important canonical problem for multiphase simulations

- No viable methods to measure secondary drop size/velocity statistics or the 3D morphology of the ring shaped ligament

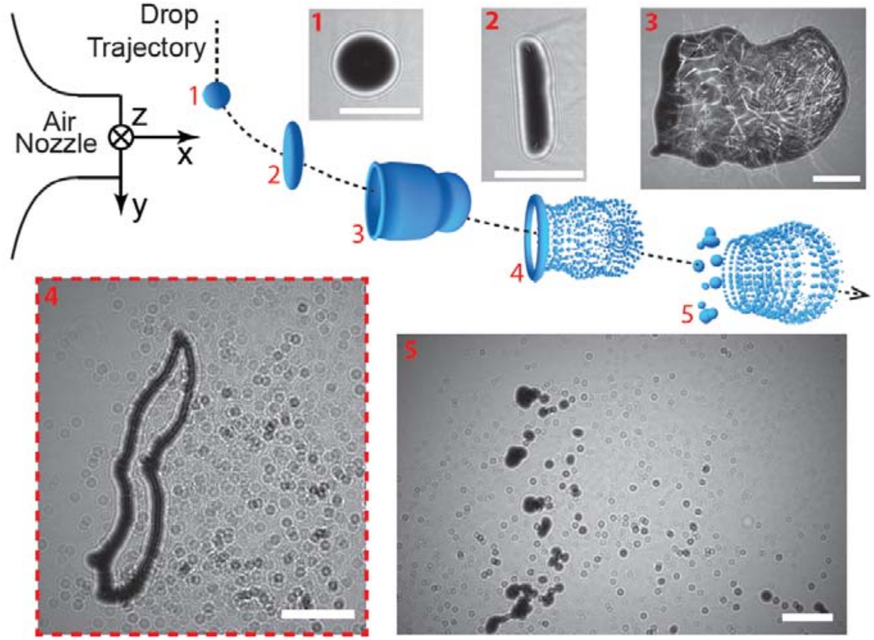


digital holograms of the breakup of an ethanol drop in an air-stream (Gao, Guildenbecher et al 2013, *Opt. Lett.*)

Experimental configuration: Double-pulsed laser and imaging hardware as typically used in PIV

- $\lambda$ = 532 nm, 5 ns pulsewidth
- Interline transfer CCD (4008 × 2672, 9 μm pixel pitch)
- Temporal separation, $\Delta t$ = 62 μs, determined by laser timing
  - Note: experiments in Guildenbecher et al, 2013, *Proceedings of Digital Holography and 3-D Imaging* confirm no loss of accuracy due to the reduced coherence length of these lasers

# Aerodynamic drop fragmentation

Sandia National Laboratories

- Secondary drop sizes/positions extracted by the hybrid method
  - Comparison with phase Doppler anemometer (PDA) data confirms accuracy of measured sizes

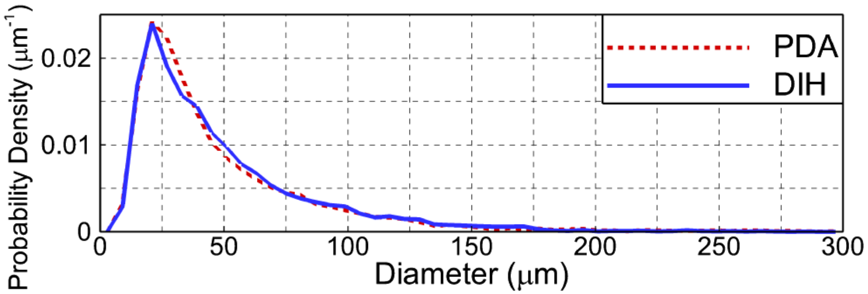


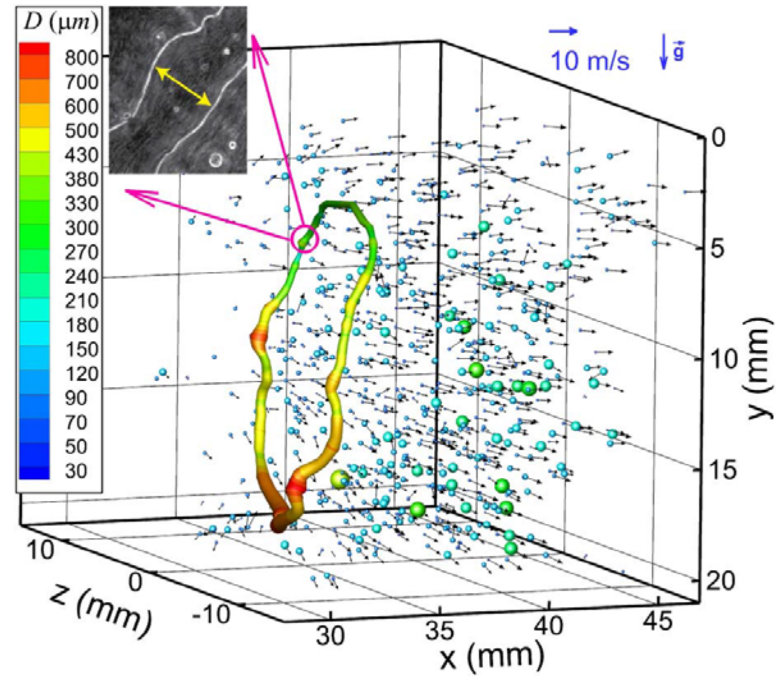


- Ring measured from *z*-location of maximum edge sharpness
  - Total volume of ring + secondary drops is within 2.2% of the initial volume
- 3C velocity measured by particle matching between successive frames
  - Expected symmetry observed with higher uncertainty in *z*-direction

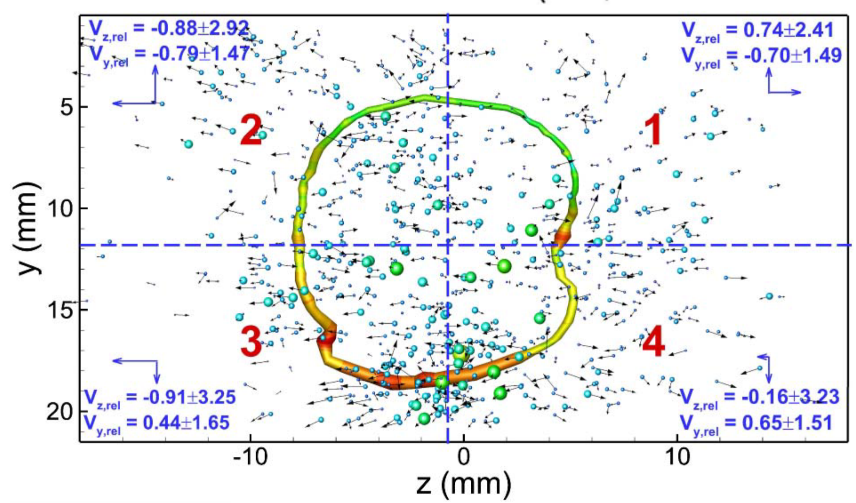

# Drop impact on a thin film

Motivation: measurement of secondary droplet by other methods requires significant experimental repetition

- Process symmetry provides opportunities to validate accuracy

Experimental configuration:

- Double pulsed laser ($\lambda$ = 532 nm, 5 ns pulsewidth)
- Interline transfer CCD (4872 × 3248, 7.4 μm pixel pitch)
- Temporal separation, $\Delta t$ = 33 μs, determined by laser timing

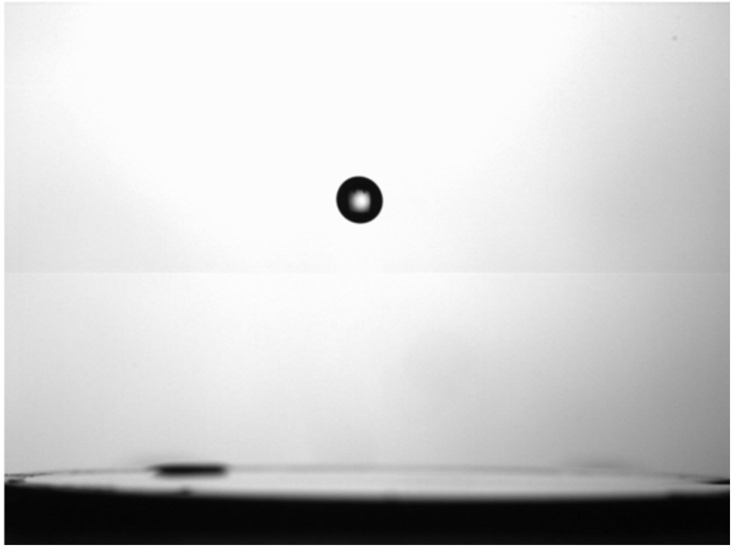

impact of a 3 mm water drop on a 2 mm water film (Guildenbecher et al, 2013, *Exp. Fluids*.)

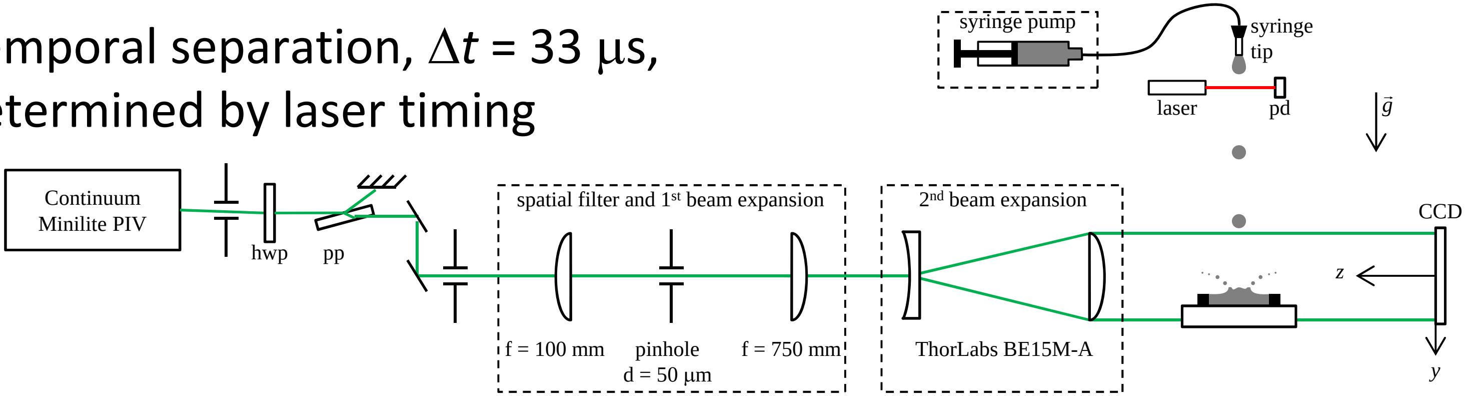


experimental configuration of holographic recording of drop impact on a thin film (Guildenbecher et al, 2013, *Exp. Fluids*.)

# Drop impact on a thin film

Sandia National Laboratories

Again processed with the hybrid method

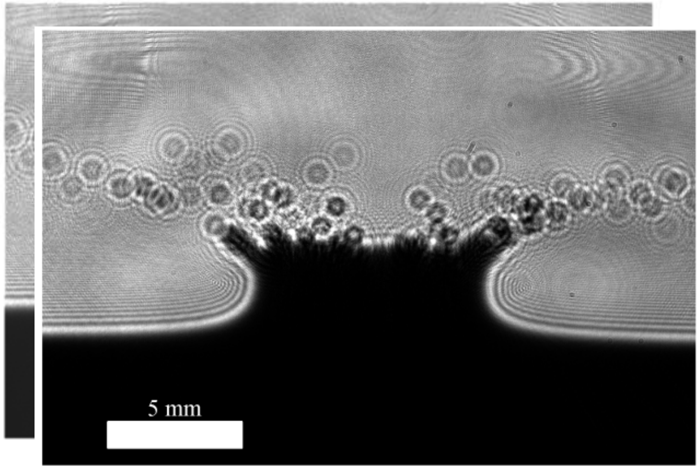


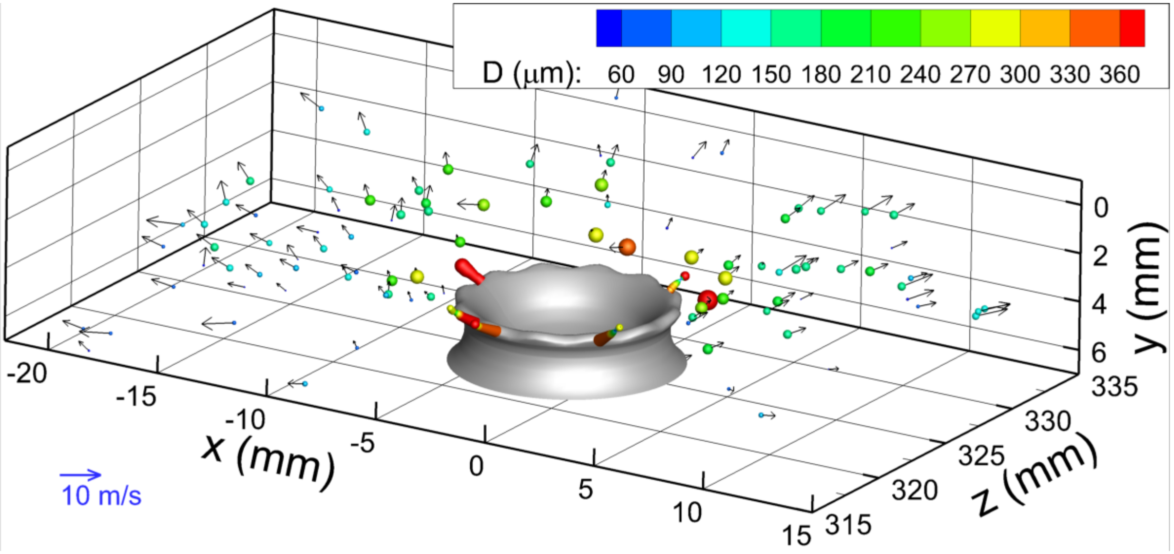


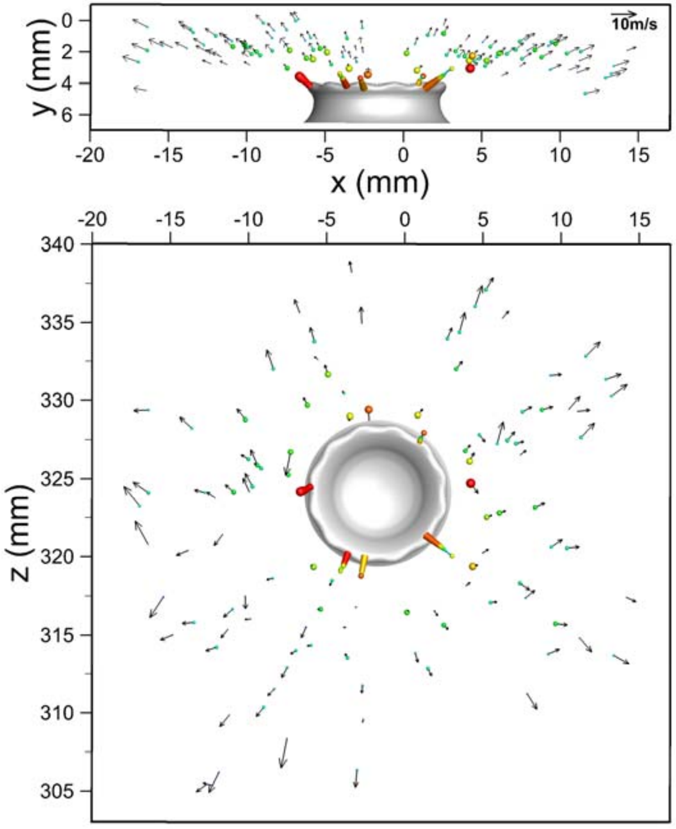


holographic reconstruction of
drop impact on a thin film
(Guildenbecher et al, 2013, *Exp. Fluids*.)

# Drop impact on a thin film

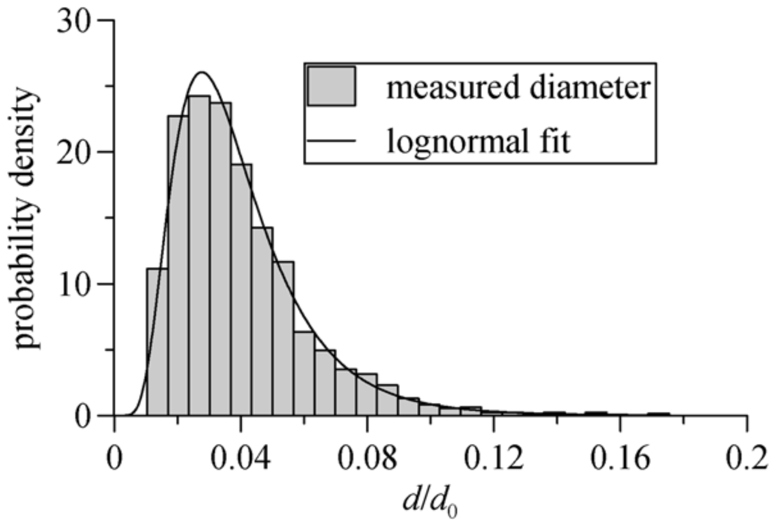


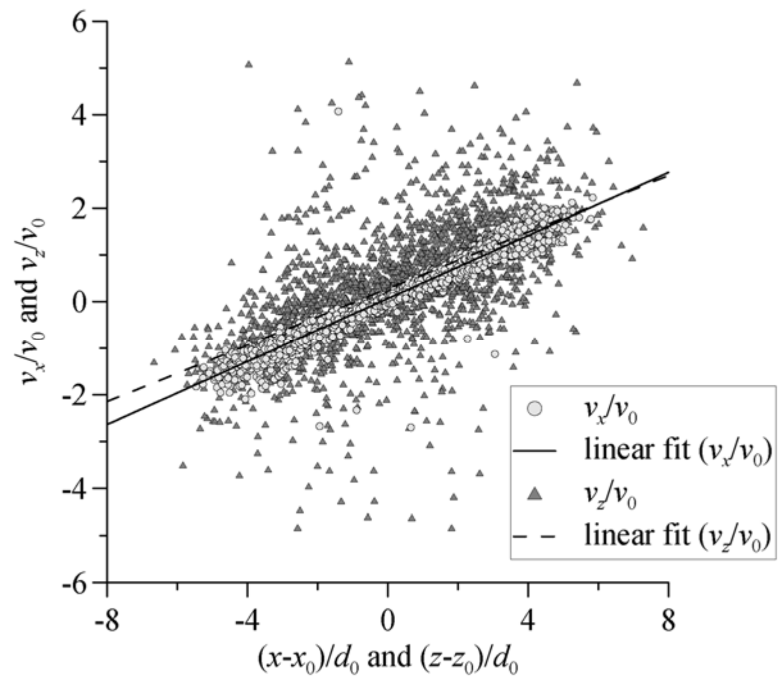


Drop size distribution shows the expected lognormal behavior

- Probability goes to zero at large and small diameters

Symmetry in the in-plane ($v_x$) and out-of-plane ($v_z$) velocities confirms accuracy in measured $v_z$

- Difference in scatter gives estimated *z*-uncertainty of $0.72 \cdot \overline{d}$

# Sonic pellets from a shotgun

<u>Motivation:</u> a shotgun simulates blast environments

<u>Challenge:</u> Shock-waves introduce noise

Holography configuration for shotgun investigations

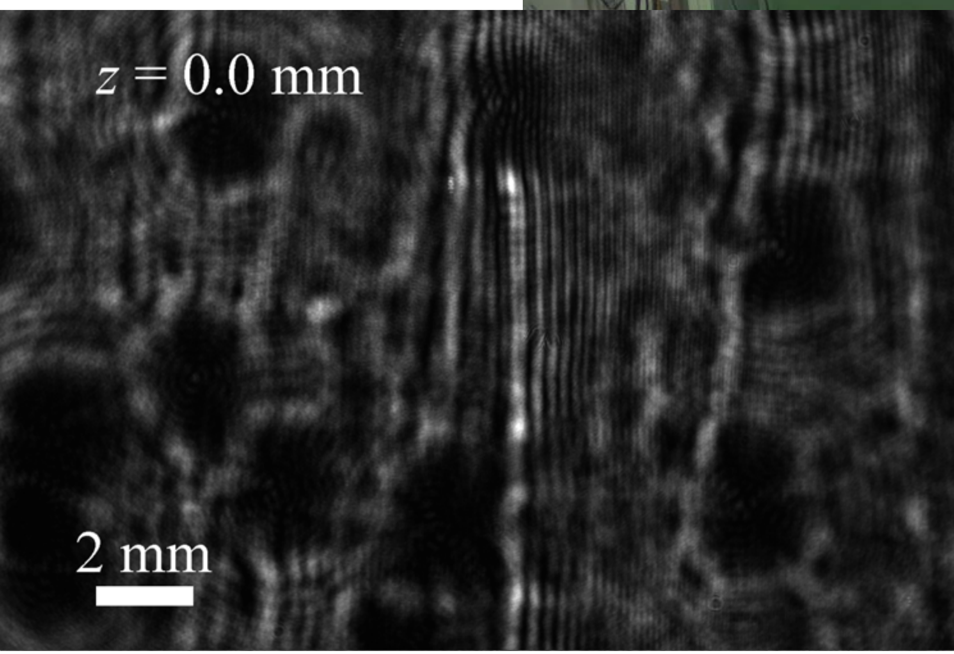


Reconstructed amplitude throughout depth, $z$

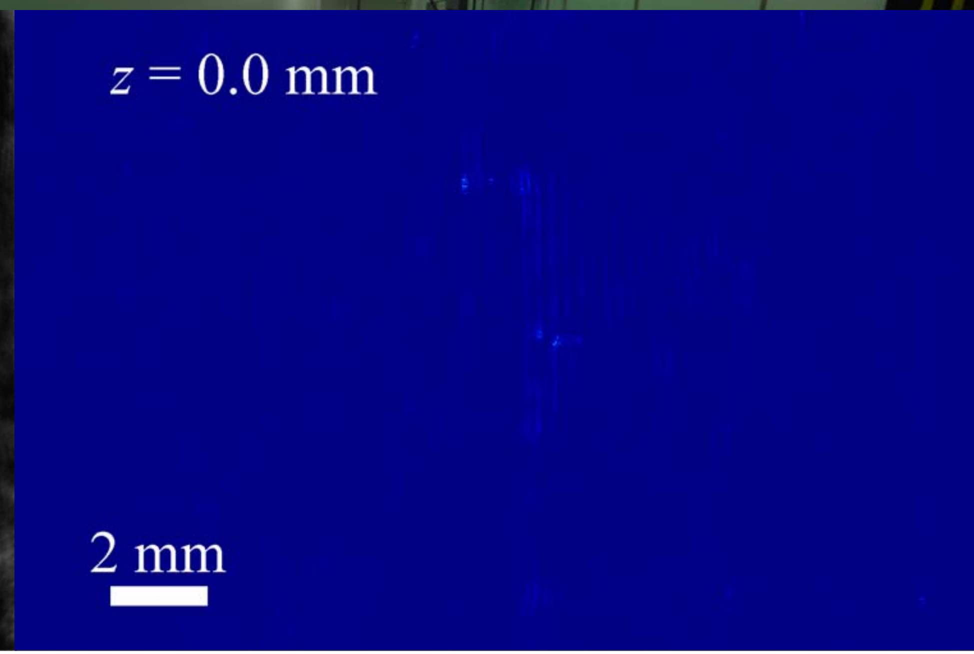


Reconstructed edge sharpness throughout depth, $z$

# Cross-correlation method

Theory: in-focus particle images from two sequential holograms contain correlated information

- The maximum cross-correlation, *c*, gives the displacement ($\Delta x$, $\Delta y$)

$$c = \max_{\Delta x, \Delta y}\left[\sum_m \sum_n \mathrm{Img}_1(m,n)\,\mathrm{Img}_2^*(m,n)(m-\Delta x, n-\Delta y)\right]$$

- $\mathrm{Img}_1$ and $\mathrm{Img}_2$ chosen as the edge sharpness images from the two frames
- $z$ positions in each frame ($z_1$ and $z_2$) are found from the maximum value of $c$ over all possible combinations of $z_1$ and $z_2$

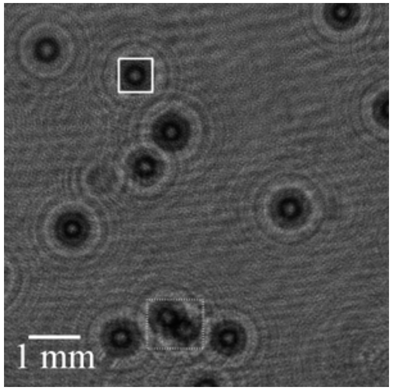


hologram (Guildenbecher et al, 2013, *Opt. Lett.*)

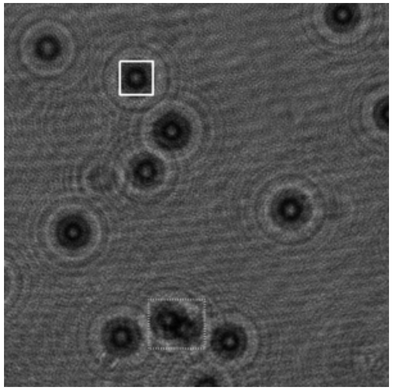

hologram after displacing the particle field by 2 mm (Guildenbecher et al, 2013, *Opt. Lett.*)

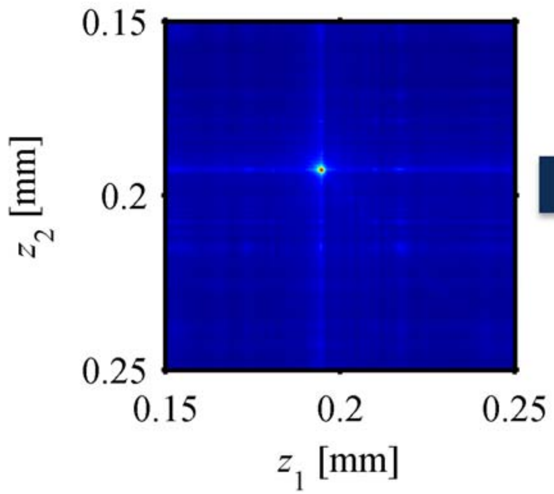


maximum value of *c* for the particle in the white boxes (Guildenbecher et al, 2013, *Opt. Lett.*)

$z_1$ = 194.72 mm,
$z_2$ = 192.72 mm,
$\Delta z$ = 2.00 mm

# Cross-correlation method

Again, experimentally validated with quasi-stationary particles in silicone oil

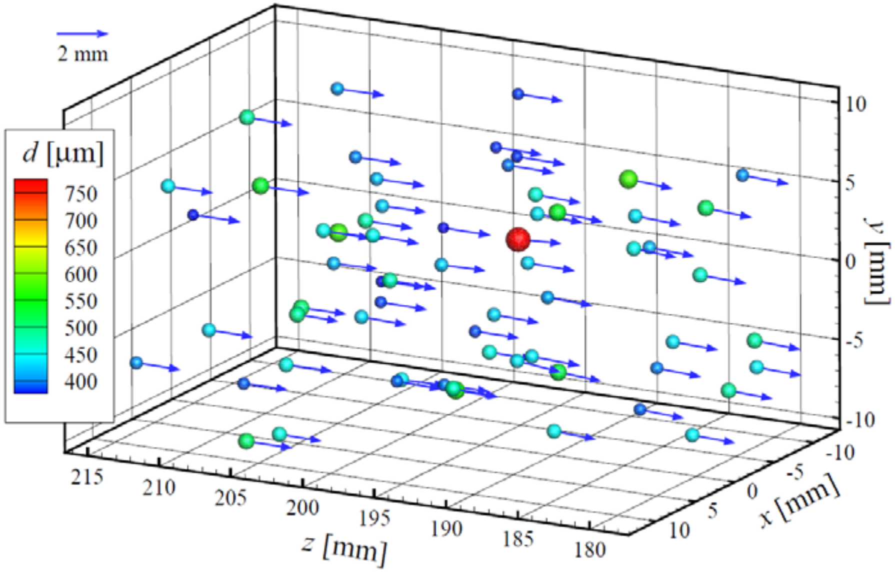


measured displacement field from one realization
(Guildenbecher et al, 2013, *Opt. Lett.*)

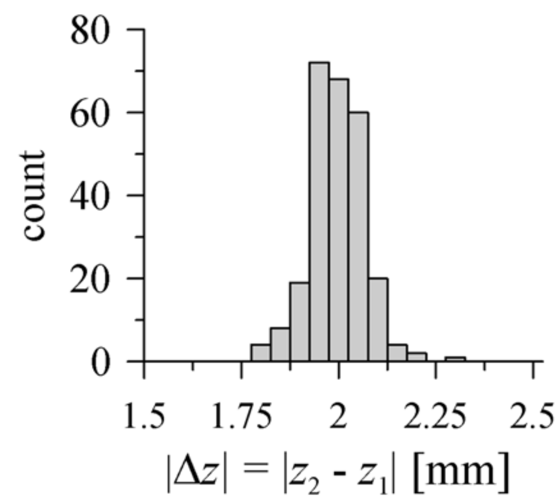


measured *z*-displacements from all realizations
(Guildenbecher et al, 2013, *Opt. Lett.*)

- Actual displacement = 2.0 mm
- Mean detected displacement = 1.996 mm +/- 0.072 mm
  - Standard deviation of 0.15 times mean diameter
  - Order of magnitude improvement compared to uncertainties in the literature

# Sonic pellets from a shotgun

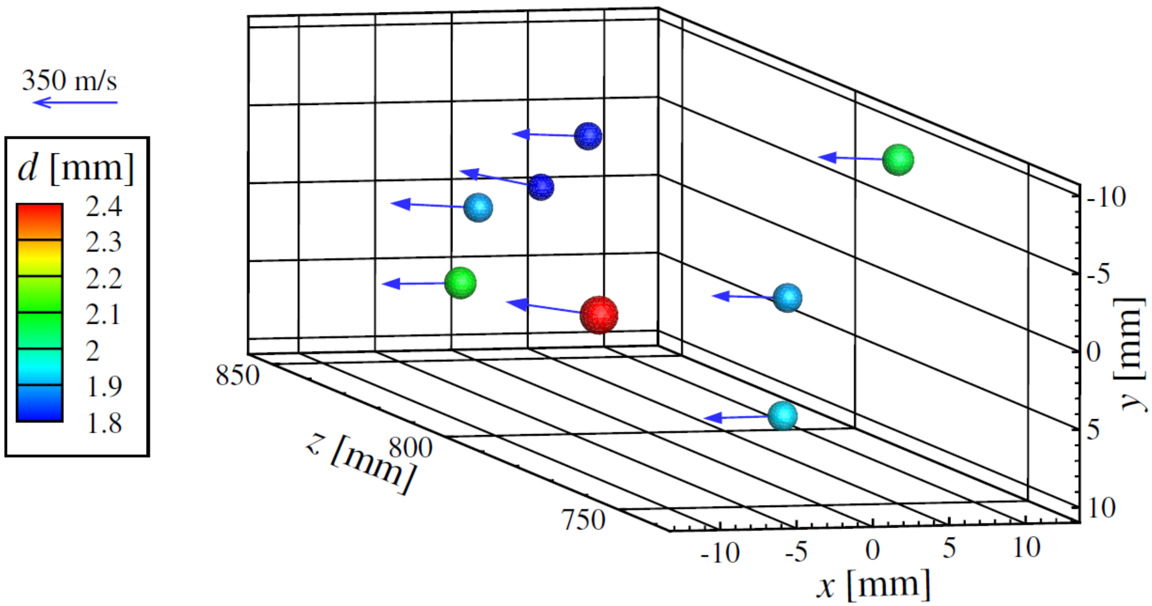


particle field from the shotgun measured with the cross-correlation method
(Guildenbecher et al, 2013, *Opt. Lett.*)

Results closely match the expected mean velocity (350 m/s) and diameter (2.0 mm)

- Uncertainty in $\Delta z$ is on the order of 0.2 particle diameters

# Fluid measurement

In particle image velocimetry (PIV) and particle tracking velocimetry (PTV), tracer particles are used to measure flow velocity

- Similar measurements can be done with digital holography

Consider: $\bar{d} \approx 465\,\mu m$ particles in 10,000 cSt silicone oil, stirred at 100 rpm by a $r$ = 1.58 mm stir rod

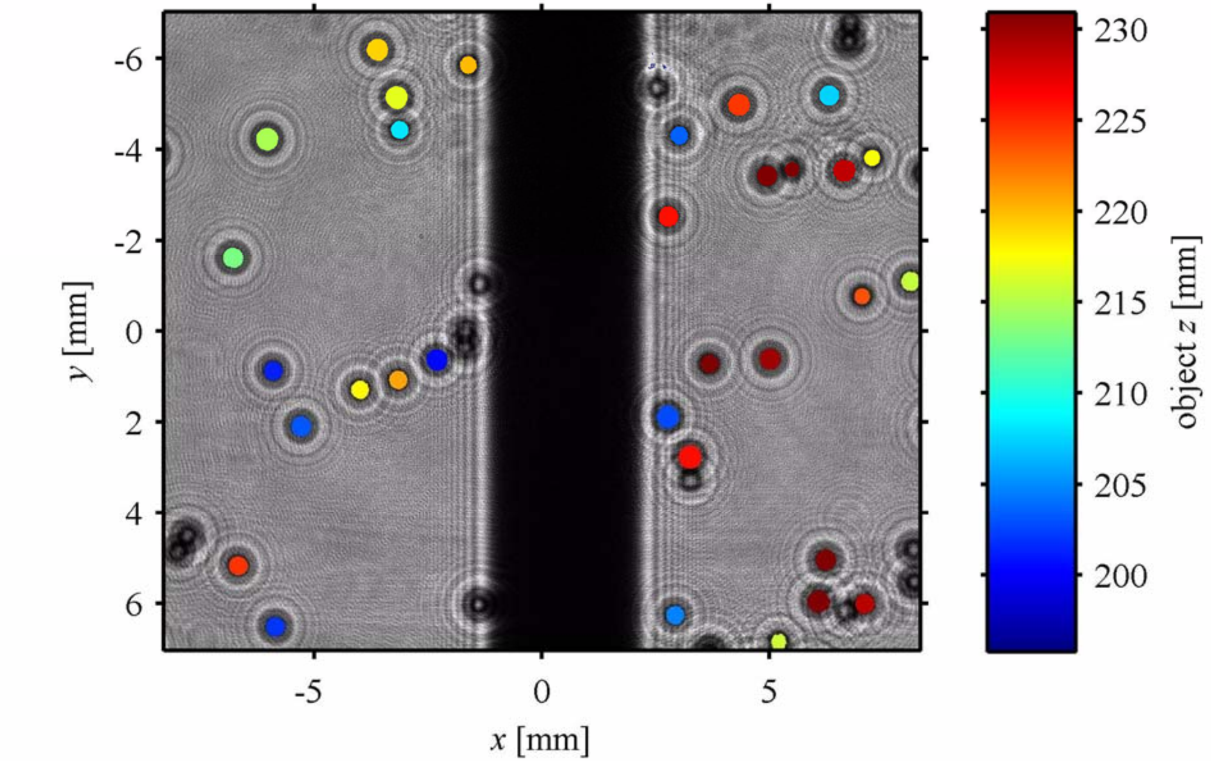


particles measured with the hybrid method, background shows the recorded hologram

# Fluid measurement

Advantages:

- Simple optical setup requiring only one line-of-sight view
- Large depth of field (hundreds of mm possible)
- Particle sizes can be measured (if desired)

Challenges:

- High uncertainty in the *z*-direction
- Particle field must be relatively spare providing only limited vectors
- Vectors at random positions
- Methods not as mature as PIV or even tomographic-PIV

**Note: the literature contains many works on holographic-PIV. My own work has not been focused on these applications**

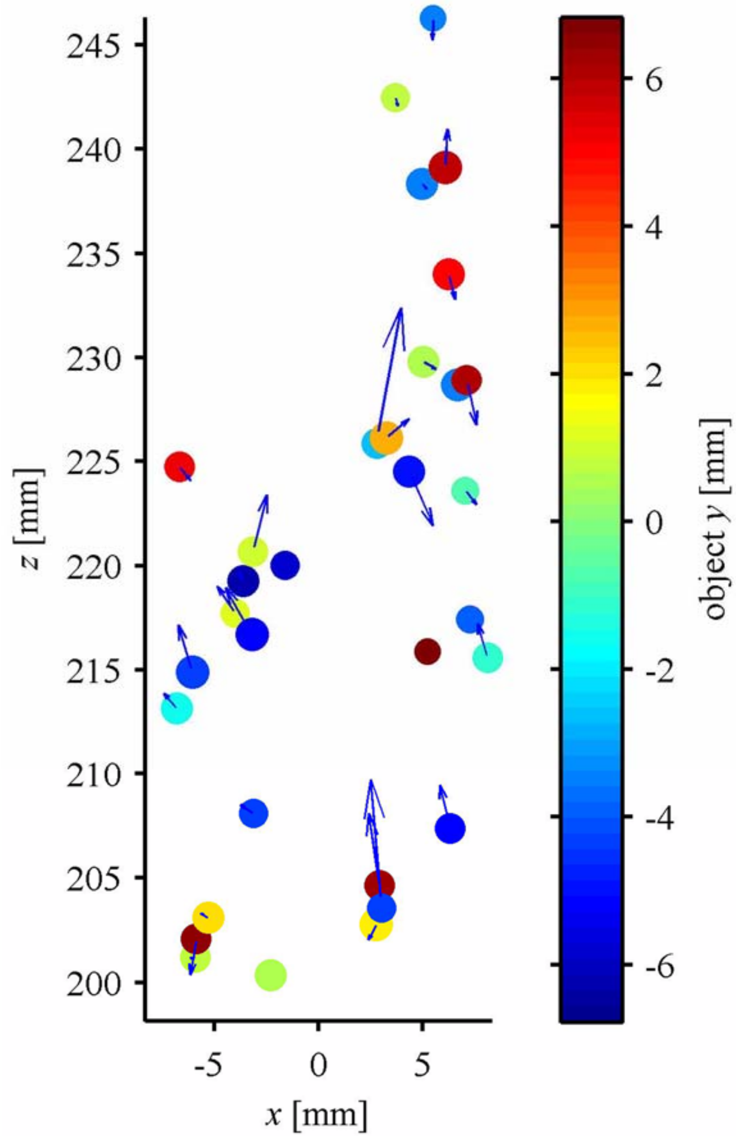

measured particles in a swirl flow, viewed in reconstructed *x*-*z* plane

# Aluminum drop combustion in propellants

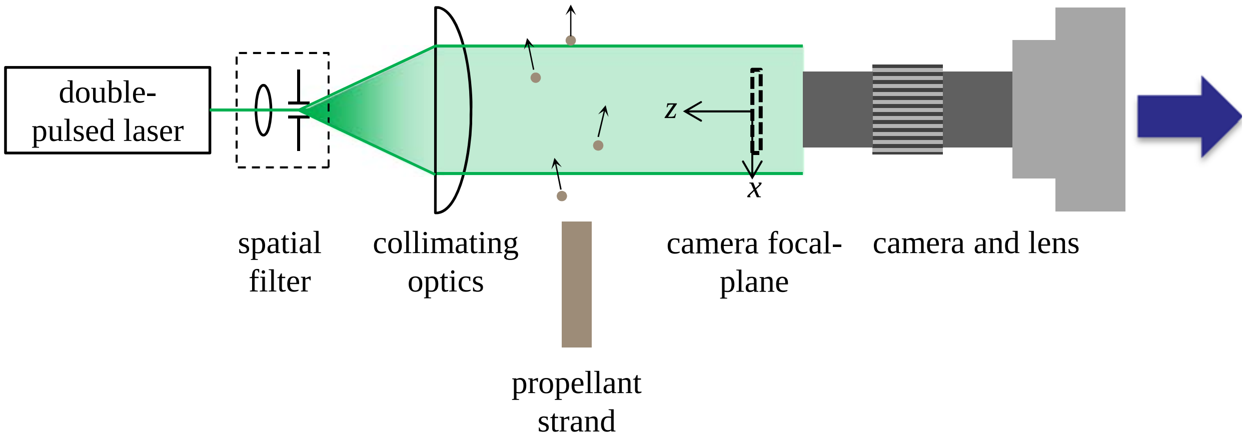


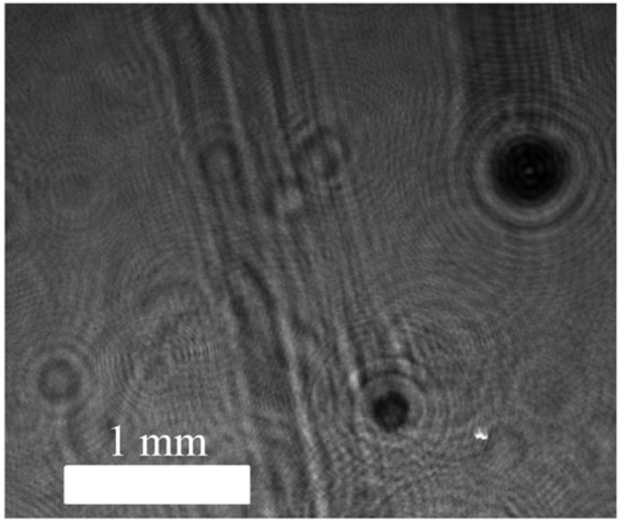


recorded hologram

<u>Propellant:</u> solid-rocket propellant pressed into a strand roughly 5 mm in diameter and initially 10 cm long

- Combusts from the top surface down, ejecting molten aluminum particles traveling on the order of 10 m/s

<u>Laser:</u> Continuum Minilite Nd:YAG, 532 nm wavelength, 5 ns pulse duration

<u>Camera:</u> sCMOS from LaVision at 15Hz

<u>Lens:</u> Infinity K2 long distance microscope with CF-4 objective

- ~ 6X magnification

# Aluminum drop combustion in propellants

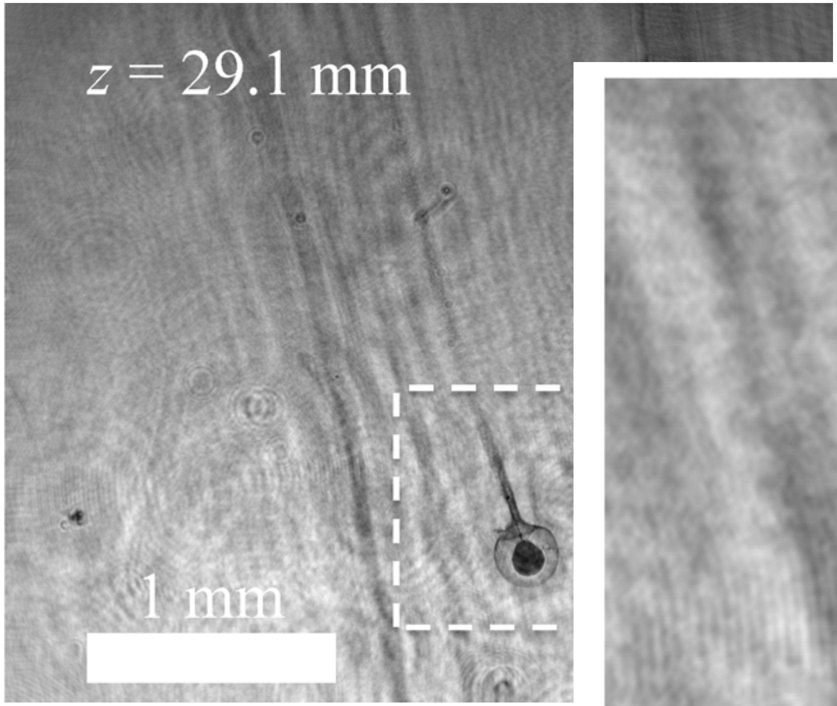


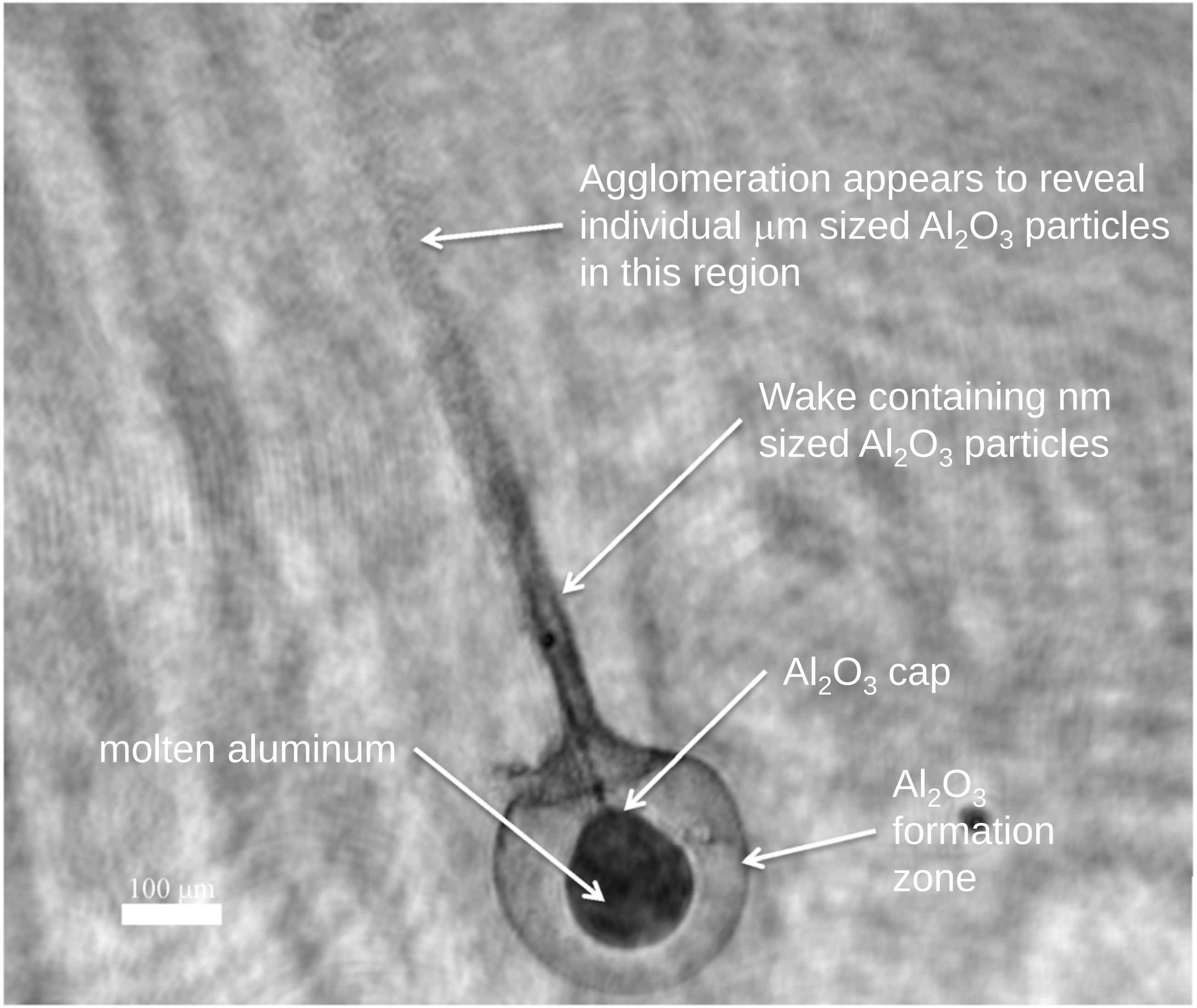

# Acknowledgements


- The work presented here is a joint effort:
  - Daniel R. Guildenbecher (1512)—ECLDRD—investigating applications to high-Weber number impact and liquid dispersion
  - Phillip L. Reu (1535)—WSEAT—considering applications to large, high-velocity shrapnel fields
- Significant thanks also goes to our collaborators at Purdue University
  - Professor Jun Chen and doctoral candidate Jian Goa
  - SNL sponsored work to develop particle detection algorithms
- Additional thanks to Thomas Grasser, Daniel Scoglietti, Lee Stauffacher, Luke Engvall, Sean Kearney, and many others….

Backup slides

# Particle extraction methods

Development focuses on:

1. Improvement and validation of the depth uncertainty
2. Reduction of “user-tunable” parameters
3. Measurement of non-spherical particles in extreme environments

Many parameters affect the accuracy:

particle size *d*, particle distance *z*, particle number density, particle shape, particle overlap, laser wavelength $\lambda$, pixel size $\Delta x$, number of pixels *N*, noise, etc…

Our development began with construction of non-dimensional recording/reconstruction models which consider as many factors as possible (Guildenbecher et al, 2013, Applied Optics)

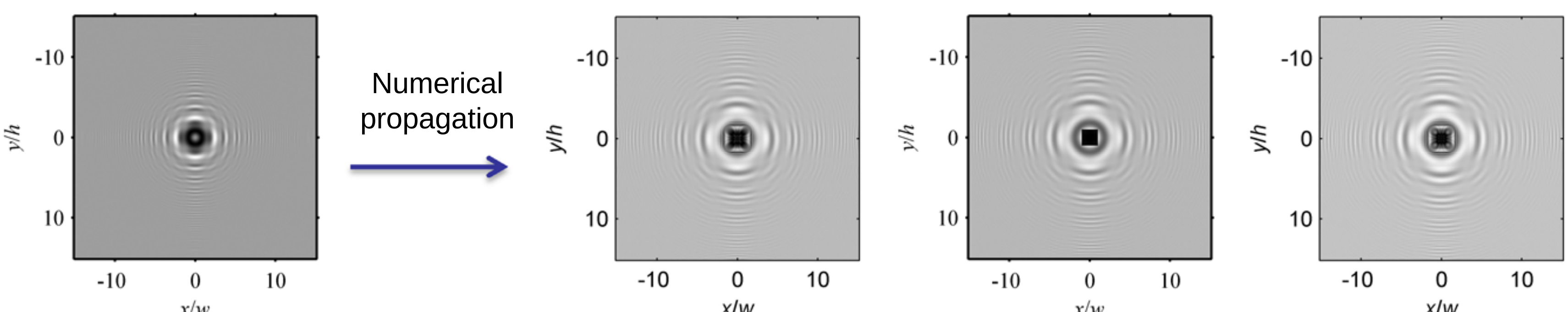


Simulated hologram of a square

Reconstruction at $Z = 0.9Z_0$

Reconstruction at $Z = Z_0$

Reconstruction at $Z = 1.1Z_0$

# Methods comparison

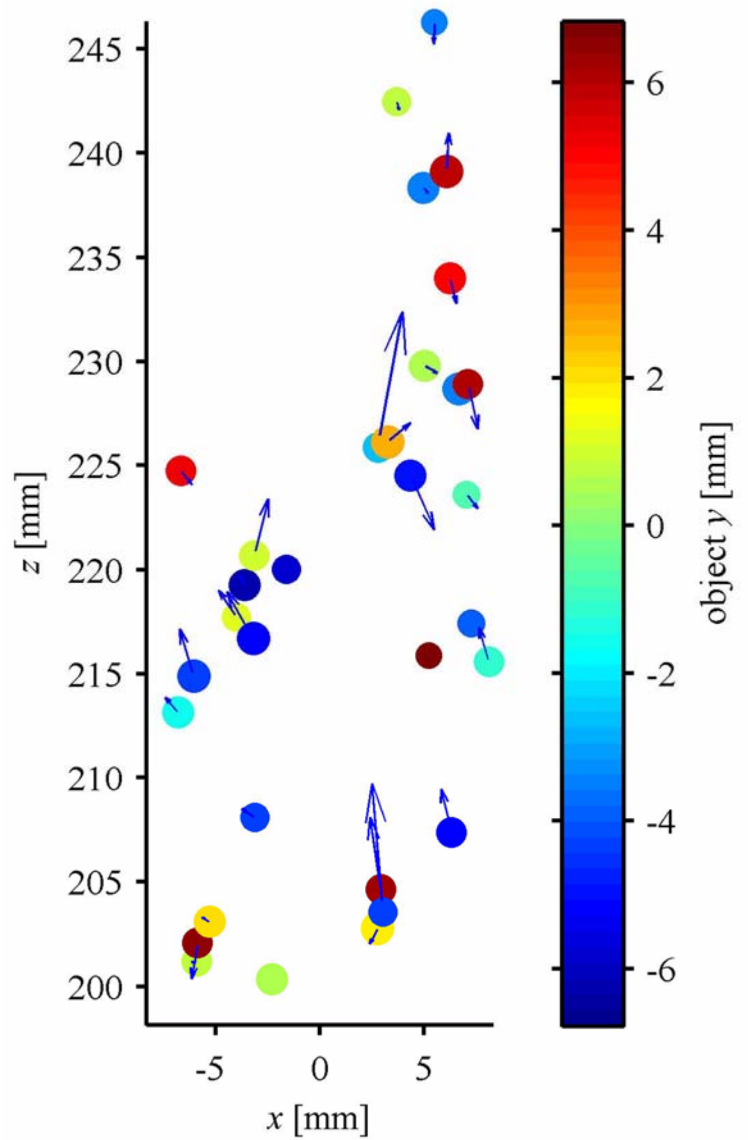


results from hybrid method

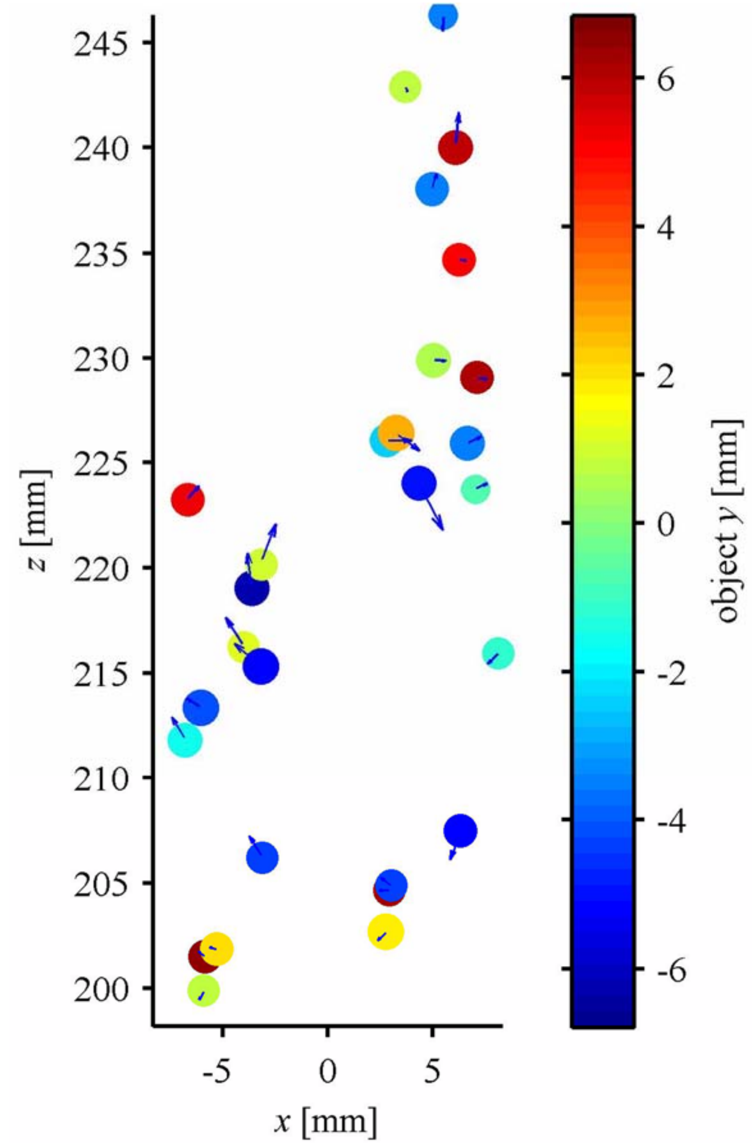


results from cross-correlation method